



HAL
open science

Mapping the structural diversity of C₆₀ carbon clusters and their infrared response

Clement Dubosq, Cyril Falvo, Florent Calvo, M. Rapacioli, Pascal Parneix, Thomas Pino, Aude Simon

► To cite this version:

Clement Dubosq, Cyril Falvo, Florent Calvo, M. Rapacioli, Pascal Parneix, et al.. Mapping the structural diversity of C₆₀ carbon clusters and their infrared response. 2019. hal-02087987v1

HAL Id: hal-02087987

<https://hal.science/hal-02087987v1>

Preprint submitted on 2 Apr 2019 (v1), last revised 9 May 2019 (v2)

HAL is a multi-disciplinary open access archive for the deposit and dissemination of scientific research documents, whether they are published or not. The documents may come from teaching and research institutions in France or abroad, or from public or private research centers.

L'archive ouverte pluridisciplinaire **HAL**, est destinée au dépôt et à la diffusion de documents scientifiques de niveau recherche, publiés ou non, émanant des établissements d'enseignement et de recherche français ou étrangers, des laboratoires publics ou privés.

Mapping the structural diversity of C₆₀ carbon clusters and their infrared response

C. Dubosq¹, C. Falvo^{2,3}, F. Calvo³, M. Rapacioli¹, P. Parneix², T. Pino², and A. Simon^{**1}

¹Laboratoire de Chimie et Physique Quantiques LCPQ/IRSAMC, Université de Toulouse and CNRS, UT3-Paul Sabatier, 118 Route de Narbonne, F-31062 Toulouse, France

²Institut des Sciences Moléculaires d'Orsay (ISMO), CNRS, Univ. Paris Sud, Université Paris-Saclay, 91405 Orsay, France

³Univ. Grenoble Alpes, CNRS, LIPhy, 38000 Grenoble, France

April 2, 2019

Abstract

The current debate about the nature of the carbonaceous material carrying the infrared (IR) emission spectra of planetary and proto-planetary nebulae, including the broad plateaus, calls for further studies on the interplay between structure and spectroscopy of carbon-based compounds of astrophysical interest. In this work, broad statistical samples of C₆₀ isomers were computationally determined without any bias using a reactive force field, their IR spectra being subsequently obtained following local optimization at the density functional based tight-binding level of theory. Structural analysis reveals four main structural families identified as cages, planar polycyclic aromatics, pretzels and branched. Comparison with available astronomical spectra indicates that only the cage family could contribute to the plateau observed in the 6–9 μm region. The present framework shows great promises to explore structural and spectroscopic features in more diverse and possibly hydrogenated carbonaceous compounds, in relation with astronomical observations.

Keyword: astrochemistry — ISM: dust — ISM: lines and bands — Infrared:ISM — Molecular processes

1 Introduction

Buckminsterfullerene (C₆₀) was recently identified in Space [7, 35]. Yet, the processes leading to its formation in circumstellar environments of carbon-rich evolved stars remain unclear [1] and two main mechanisms have been invoked so far. In the bottom-up mechanism, fullerenes grow from successive reactions between carbon chains and small molecules, as possibly found in the hot and dense envelopes of evolved stars. Alternatively, in low-density environments such as interstellar clouds the so-called top-down mechanism could take place [3] with larger carbon grains or dehydrogenated polycyclic aromatic hydrocarbons (PAHs) [2] progressively rearranging into fullerenes under the action of ultraviolet photons or by collisions with energetic particles.

Recent observational studies have suggested that fullerenes could be produced by photochemical dehydrogenation and isomerization of amorphous carbon grains [14, 13, 15, 16], although the composition of such grains is still debated. Infrared (IR) spectroscopic observations of fullerene-rich planetary nebulae (PNe) found a broad plateau with substructure in the 6–9 μm [14, 13, 15, 16, 1]. The origin of this plateau remains elusive and various hypotheses were made on its possible carriers, including hydrogenated amorphous carbon (HAC) compounds [1], very small grains or PAH clusters [42, 5, 30]. Similarly, the 8 and 12 μm plateau features of some proto-planetary nebulae (PPNe) were assigned to the vibrations of alkanes or alkyl side groups pertaining to large carbonaceous particles [24, 19], whose details also remain unclear.

These observations and their various interpretations call for further studies about the nature of the potential carriers of these spectral features. The present Letter describes a purely computational framework designed to

*Corresponding author: aude.simon@irsamc.ups-tlse.fr

systematically explore the structural diversity of C_{60} isomers in a statistically unbiased way and to relate the various isomers to IR spectral features. Sorting these isomers using appropriate order parameters, our mapping provides unprecedented correlations between structure and spectroscopy which, in turn, could give insight into the possible formation mechanisms of fullerenes in astrophysical environments.

In Section 2, we briefly describe the different computational approaches. Section 3 analyses the structural diversity for C_{60} , their mapping into four main families of isomers and the relation with IR features. Section 4 compares the calculated IR spectra with astronomical data available for selected PNe and PPNe. Some concluding remarks are finally given in Section 5.

2 Computational details

A systematic and unbiased search for isomers of C_{60} was computationally undertaken using the efficient but realistic REBO reactive force field [4]. Replica-exchange molecular dynamics (REMD) simulations were performed in the 2500-6500 K temperature range using 16 trajectories, the temperatures being allocated in a 12-long geometric series with 4 extra temperatures at 3342.4, 3440.6, 3645.7, 3752.8 K around the C_{60} melting temperature [22]. All replicas were initiated from the buckminsterfullerene global minimum and the trajectories were integrated over 100 ns using a time step of 0.1 fs. Configurations were periodically saved and locally reoptimized using the REBO force field. Spherical boundary conditions were used and the density was varied over 4 different simulations with $\rho = 0.025, 0.15, 0.4, \text{ and } 1.7 \text{ g.cm}^{-3}$. Dissociated structures corresponding to a threshold distance larger than 1.85 Å were excluded. This unbiased sampling stage produced 656438 nonequivalent isomers.

While REBO provides a reasonable description of intramolecular forces in carbon nanostructures, a chemically more accurate description was then employed to refine the structures, evaluate their relative energies and determine their infrared spectra in the harmonic approximation. The self-consistent charge (SCC) density-functional based tight-binding (DFTB) method [29, 10, 11] employing the mio set of parameters [10] with additional dispersion correction [32] was used for this purpose. Although significantly more expensive than REBO, the SCC-DFTB approach remains computationally efficient due to the use of approximations and pre-computed pair integrals. It was successfully employed to determine structural [45, 44, 43, 26], spectroscopic [21, 37, 39, 41, 40], and fragmentation [38, 36, 31] properties of PAH molecules and oligomers of astrophysical interest under various charge and energy states, at and away from equilibrium. The formation of PAHs or carbon clusters [34, 33] and their hydrogen uptake capability [8] were also investigated by SCC-DFTB with molecular dynamics.

Reoptimization of the REBO isomers eventually produced 309168 independent structures at the SCC-DFTB level of theory, for which the IR absorption spectra were computed in the double harmonic approximation. The raw frequencies of the vibrational modes obtained with SCC-DFTB were corrected using affine laws in order to match best reference data (see Appendix A). The coefficients of these corrections depend on the frequency domain. This results in discontinuity near 6.0 μm , preventing from an accurate analysis of the [5.8-6.2 μm] domain, which is a limitation of the present work.

All REBO simulations were performed using the LAMMPS software package [28], the SCC-DFTB calculations being carried out with the deMonNano code [17].

3 Structural partitioning

The structural properties of our sample of 3×10^5 isomers were unveiled by employing a reduced number of parameters that characterize features at local or more global scales. Besides the energy itself, we considered the shape of the individual isomers through the Hill-Wheeler indices I_0 , β and γ obtained by expressing the three momenta of inertia $I_1 \geq I_2 \geq I_3$ as $I_k = I_0 \{1 + \beta \sin[\gamma + (4k - 3)\pi/6]\}$ for $k = 1-3$ [18]. Here $I_0 > 0$ measures the overall spatial extension of the isomer, and is related to the gyration radius r_g as $I_0 = 2r_g^2/3$ up to a mass factor. $\beta < 1$ denotes the asphericity parameter, or the extent of deviation to the perfect sphere for which $\beta = 0$. Finally, the triaxiality parameter γ measures the nature of the equivalent ellipsoid, its oblate or prolate character. As will be shown below, the Hill-Wheeler parameters, previously used to characterize the shape of metallic clusters [6], appear to be quite sensitive for carbon compounds as well. In practice, we focus on the radius of gyration and the asphericity parameters, leaving the triaxiality parameter aside.

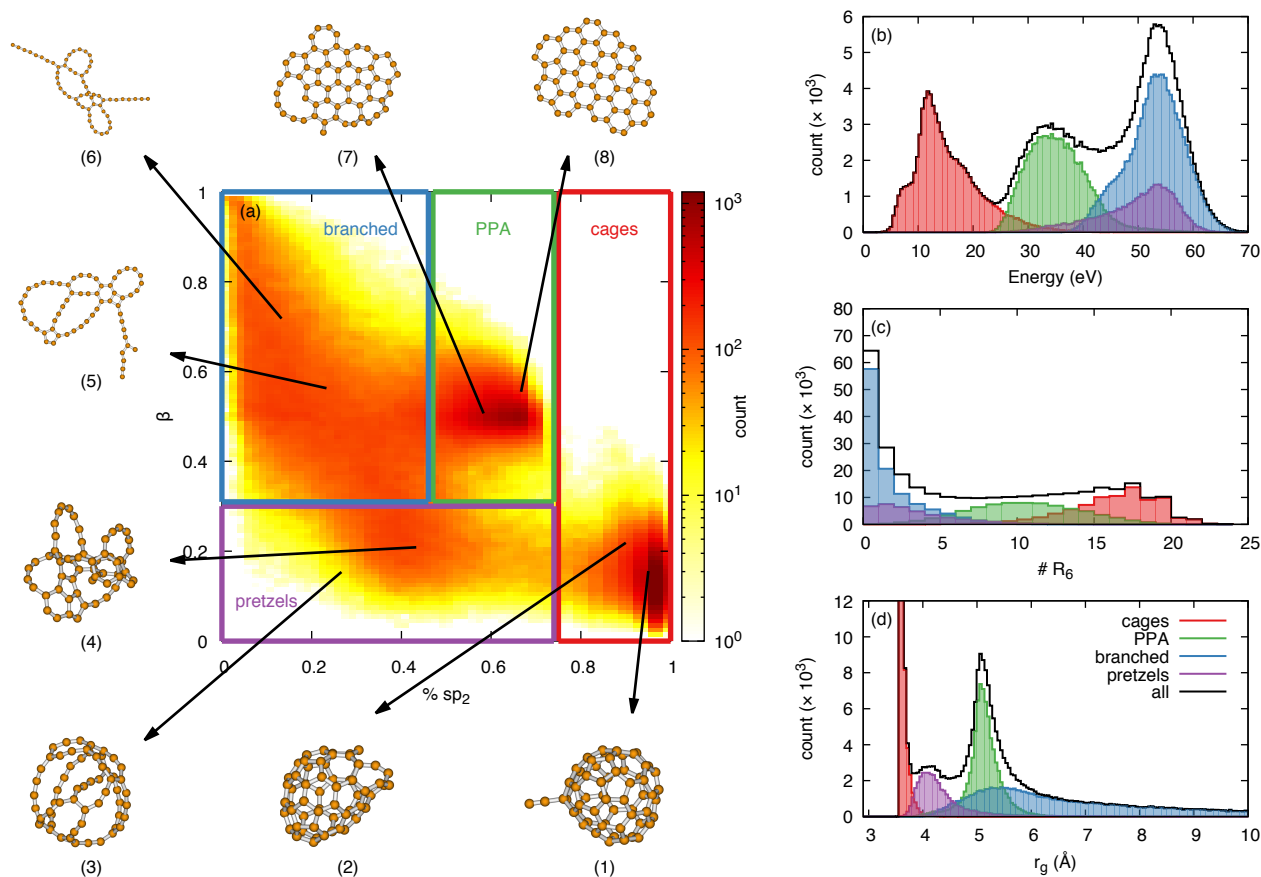


Figure 1: Probability distributions of the samples of isomers based on specific order parameters. (a) Two-dimensional distribution as a function of the sp^2 fraction and asphericity β . Panels (b), (c), and (d) show the one-dimensional distributions as a function of isomer energy, number of 6-membered cycles, and gyration radius, respectively. In panel (a) the boxes define the four structural families denoted as cages, PPA, pretzels, and branched, respectively, with the same colors being used in panels (b-d). Two examples of structures numbered (1-8) are depicted for each family.

Local order in the carbon nanostructures was scrutinized from the hybridization level. From the SCC-DFTB electronic density matrix, Mayer's bond orders [27] were computed and bonds placed accordingly when the bond order was higher than 0.8. A carbon atom with a coordination number of $n + 1$ is attributed to a sp^n hybridization level. Eventually, an average fraction of sp^2 hybridization was retained as the main local order parameter to measure the extent of sp^2 within a given isomer.

A last discriminatory parameter, which can be seen as a semi-local or semi-global index, is the number of 6-membered rings within each isomer. This quantity is related to the extent of connectivity within the structure, and can also differentiate isomers with large aromatic domains from those having topological defects.

Figure 1 shows how the various order parameters are distributed among the 3×10^5 isomers.

Among the five parameters considered, the fraction of sp^2 atoms and the asphericity β are found to discriminate best the various isomers into structural families. Four such families are identified as fitting into rectangular boxes in Fig. 1(a). Each of these families also has generally clear signatures as well-defined peaks in the one-dimensional distributions of Figs. 1(b-d) as a function of energy, number of 6-membered cycles, and gyration radius, respectively.

The first family, which is thermodynamically the most stable (lowest energies), is defined by isomers with the highest fraction of sp^2 atoms (above 75%). They generally show a high spherical character (low β). These isomers also have the highest number of 6-membered rings, but the lowest gyration radius (3.7 Å) indicating a rather compact shape. These 8.2×10^4 isomers are referred to as cages, and they include buckminsterfullerene as their most remarkable member.

In order of increasing energy, the second family consists of intermediate fractions of sp^2 atoms comprised between 45% and 75%, and an asphericity parameter β higher than 0.3. These isomers exhibit a clear peak in the

energy and gyration radius distributions, and once resolved they also show intermediate values in the number of 6-membered rings. This family denoted as planar polycyclic aromatic (PPA) contains 7.7×10^4 members.

One minor peak in the gyration radius distribution near 4 \AA points at a specific family with rather compact structures, correlated with low asphericity but more arbitrary sp^2 fraction (still lower than 75%). This third family is defined in the two-dimensional distribution from $\beta < 0.3$, and comprises rather spherical but fairly open structures with many carbon chains. Following [22] we denote the 3.8×10^4 members of this family as pretzels.

Finally, all the remaining isomers lie in the range of $\beta > 0.3$ and with a sp^2 fraction lower than 45%. They are associated with the highest energies, the lowest number of 6-membered rings, but the highest gyration radius, whose distribution is particularly broad. They usually contain multiple linear chains connected at a limited subset of atoms. This family is broadly referred to as made of branched structures, which are found in numbers of 1.1×10^5 .

Visual depiction of selected isomers was also added in Fig. 1 to further justify the terminology employed above. For each family, the statistically averaged values of all the five energetic or structural parameters was determined, and the Euclidean distance of each member of the family to this five-dimensional point calculated. The member having the lowest distance was identified as a most representative isomer of the family, without any bias from human judgment. The structures numbered (1), (4), (5), and (7) in Fig. 1 are these statistically most representative isomers. For each family one other isomer was chosen to further illustrate the structural diversity within the families. These isomers are numbered (2), (3), (6) and (8) in Fig. 1.

4 IR spectra in comparison with astronomical data

The IR spectra for the four structural families were obtained by summing the individual contributions from each member with a uniform weight within the families. Such a uniform distribution obviously ignores the thermodynamics, however our purpose is not to describe realistic rearrangement mechanisms but only to derive general trends relying structure with spectroscopy. For comparison with astronomical data, the IR absorption intensities were further convoluted by a Planck blackbody radiation law at 400 K, as proposed earlier by Draine and Li [9]. The four spectra thus determined for the four families are shown in the bottom part of Fig. 2.

Before comparing the calculated and observed spectra, several comments can be made on the spectra computed for the different families. All families exhibit features below $6 \mu\text{m}$, although significantly attenuated by the convolution with the Planck law for the cages population. These lines involve sp^1 carbon atoms found in surface (cages) or edge (PPA) defects, long loops and linear chains (pretzels and branched). The latter terminating chains, in particular, display a strong absorption near $4.7 \mu\text{m}$. While such isomers exist among the cage [see e.g. Fig. 1(1)] and PPA [see e.g. Fig. 1(7)] populations, they are far more numerous in more open structures such as pretzels and obviously the branched family, for which this peak is even more intense and doubled with another feature at $5.1 \mu\text{m}$.

Above $6 \mu\text{m}$ the spectral features are due to the CC stretching of sp^2 carbons that are involved in multiple 5-, 6-, or 7-membered rings. The corresponding active spectral region is broad and overlaps with the range where CCC in-plane bending modes are found near $10.5\text{--}12.5 \mu\text{m}$. Such features are most prominent for the cages population, for which the averaged spectrum exhibits a broad band between 6.2 and $11.6 \mu\text{m}$ with a sharp blue tail and a smooth red tail and a sharper maximum near $6.6\text{--}7.9 \mu\text{m}$. Finer peaks near 8.9 and $10.3 \mu\text{m}$ mark the resonance of CC stretching modes, while the band near $12.5 \mu\text{m}$ is assigned to in-plane CCC bending modes leading to some rotation of the rings. Bands located above $14 \mu\text{m}$ correspond to softer deformation modes of the carbon skeleton that are of a more collective character. The accuracy of these lines is more disputable at the present level of theory (see Appendix A.2, Table A.1), and the narrow intense band appearing near $15.7 \mu\text{m}$ should actually be shifted by $+1.2 \mu\text{m}$.

The IR spectrum obtained for the PPA family shows a very broad band extending from 6.4 to $13.3 \mu\text{m}$, with maxima at 7.4 , 9.5 , and $10.8 \mu\text{m}$. These features are the signature of CC stretching modes that also increasingly combine with CCC bending modes as the wavelength increases. Two bands near 16.4 and $21.9 \mu\text{m}$ are assigned to in-plane and out-of-plane deformation modes, respectively.

In comparison with cages and PPA isomers, the spectrum of the pretzel isomers above $6 \mu\text{m}$ displays fewer bands except broad maxima near 7.3 and $15.3 \mu\text{m}$ that we assign to CC stretchings and in-plane bendings, respectively. The much greater structural diversity among this population explains why the resonance of these

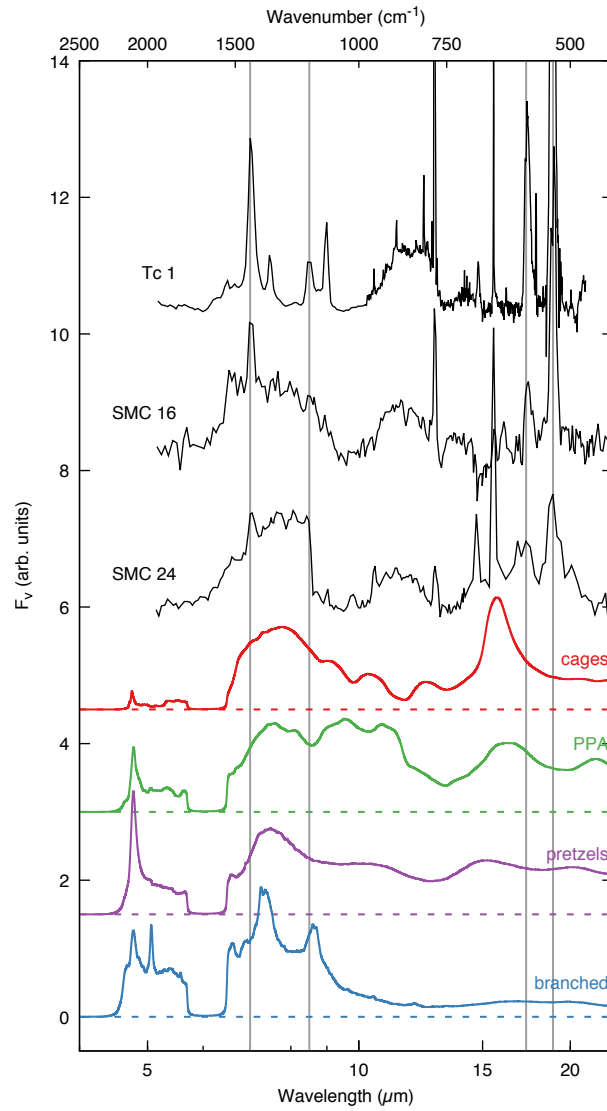


Figure 2: *Spitzer* astronomical data observed for the Tc 1 and SMP SMC 16 [14] and SMP SMC 24 [15] planetary nebulae (black curves) and IR spectra calculated for the four different families of cages, PPAs, pretzels and branched structures (red, green, purple and blue curves, respectively). The four vertical lines mark the IR active lines of buckminsterfullerene [23]

modes leads to broader bands.

Finally, the spectrum of the branched family exhibits an active region in the 6.4–9.6 μm range but hardly any feature above this range. The maxima at near 7.3 and 8.6 μm are assigned to CC stretches coupled to in-plane CCC bending modes involving sp^2 carbons that pertain both to small rings and long loops or linear chains.

We can now compare these spectra to astronomical observations recorded in C-rich and H-rich PNe of the Small Magellanic Cloud (SMC), where fullerenes and PAHs were both detected [14]. The emission features in SMP SMC 16 found in the 6–9 μm and 15–20 μm ranges possibly match those found for the cages population, given that the band calculated at 15.7 μm should be shifted by about +1.2 μm . However, the contribution of cages to the 10–13 μm plateau is more questionable. So is the presence of PPA structures, whose spectral feature near 6–10 μm is much broader than the observed data, with no remarkable feature in the 10–13 μm range either. Similarly, pretzel isomers cannot explain the astronomical data for this PNe. In contrast, we find some similarities in the spectrum of the branched family near 6–9 μm , and especially its peak at 8.6 μm . However, the branched family spectrum shows no feature above 10–13 μm , in contradiction with observations.

Comparing now the calculated spectra with the astronomical observations of the Tc 1 PNe where C_{60} and C_{70} were detected [7], the most stable cage population may also contribute to the same regions as for SMP-SMC 16 but cannot account for the very intense 10–13 μm plateau. The contribution of the other families must probably be excluded as they are too dissimilar with astronomical data for this PNe.

Comparison can also be made for the spectrum of SMP SMC 24, which was suggested to be due to a complex mixture of aliphatic and aromatic compounds such as HACs, PAH clusters, fullerenes and small dehydrogenated carbon clusters [15]. As was the case for SMP-SMC 16, only the cage family is compatible as a potential contributor to the features near 6–9 μm and 15–20 μm .

Finally, emission spectra of proto-planetary nebulae that represent the short evolutionary phase between AGB stars and PNe are also worth considering in our comparison, and here we take the example of IRAS 222725435 PPNe whose spectrum can be found in Fig. 3 of [24]. Interestingly, no intense band is observed at 4.7 μm , which excludes compounds with long carbon loops or linear carbon chains such as pretzels or members of the branched family. The features near 8 and 12 μm that were assigned to the vibrations of alkanes or alkyl side groups pertaining to large carbonaceous particles [24] have no direct counterpart on our spectra. However, the shape of the 5–8 μm feature reported by [24] is consistent with the spectrum obtained here for the cages population. Moreover, other features such as the intense band near 17 μm are not observed in PPNe. It is likely that for such PPNe hydrogenation state plays an important role in these IR features.

5 Conclusions

Fullerenes identified in Space necessarily originate from complex chemical rearrangements that proceed either by growing smaller scale species, or by reducing larger compounds until these aromatic cages show their special stability. In order to elucidate the possible intermediates in such reactions, and without assuming any specific formation mechanism, we have attempted to systematically sample the possible isomers a connected set of 60 carbon atoms can exhibit. In this purpose an efficient exploration of the conformational landscape was achieved by combining the reactive REBO force field within replica-exchange molecular dynamics simulations at temperatures as high as 6500 K, thus ensuring high energy isomers are visited and isomerization barriers are crossed. Using the more accurate SCC-DFTB method, the energies were refined and the IR spectra determined in the harmonic approximation.

Different energetic, structural and electronic parameters allowed the 3×10^5 structures thus obtained to be partitioned unequivocally into four main families denoted as cages, planar polycyclic aromatics, pretzels, or branched. The IR spectra of these families exhibit significant differences among each other, which in turn could be exploited to get insight into their potential presence in planetary and proto-planetary nebulae. Comparison between calculated and astronomical spectra generally indicates that cage isomers with their clear feature in the 6–9 μm range are relevant as possible carriers, whereas more disordered structures containing long carbon loops or a greater amount of linear carbon chains are less likely. Moreover these pretzel and branched families were found to exhibit an intense feature near 4.7 μm that has not been observed in PNe and PPNe.

This work paves the way to more systematic computational investigations of the interplay between structural and IR spectroscopic features in a greater diversity of carbonaceous clusters, possibly containing hydrogen or

other heteroatoms, at other sizes and other charge states. Obviously such a richer chemistry will require further refinements in our description of both the potential energy surfaces and the IR spectra, a more realistic account of anharmonicities being likely to play a role at higher temperatures and in chain-rich isomers. Hopefully such an unbiased exploration should help identify the structural patterns responsible for the so far unexplained astronomical spectral features of PNe, notably in the 9-13 μm region.

acknowledgements

We acknowledge the computing mesocenter CALMIP "Unité Mixte de Service du CNRS" (UMS CNRS 3667) in Toulouse for generous allocation of computer resources (p0059). We also thank Dr D.A. García Hernández for discussions related to the astrophysical relevance of this work. This work was funded by the Agence Nationale de la Recherche (ANR) project PACHYNO "Probing the diversity of Astrophysically relevant Carbon and Hydrogen Nanoparticles" ANR-16-CE29-0025, with support from the French research network EMIE (Edifices Moléculaires Isolés et Environnés, GDR 3533 of CNRS).

References

- [1] J. Bernard-Salas, J. Cami, E. Peeters, A. P. Jones, E. R. Micelotta, and M. A. T. Groenewegen. On the Excitation and Formation of Circumstellar Fullerenes. *The Astrophysical Journal*, 757:41, September 2012.
- [2] O. Berné, J. Montillaud, and C. Joblin. Top-down formation of fullerenes in the interstellar medium. *Astronomy and astrophysics*, 577:A133, 2015.
- [3] Olivier Berné and A. G. G. M. Tielens. Formation of buckminsterfullerene (C-60) in interstellar space. *Proc. Natl. Acad. Sci. U.S.A.*, 109:401, 2012.
- [4] Donald W. Brenner, Olga A. Shenderova, Judith A. Harrison, Steven J. Stuart, Boris Ni, and Susan B. Sinnott. A second-generation reactive empirical bond order (rebo) potential energy expression for hydrocarbons. *J. Phys. Cond. Matt.*, 14:783, 2002.
- [5] RH Buss Jr, AGGM Tielens, M Cohen, MW Werner, JD Bregman, and FC Witteborn. Infrared spectra of transition objects and the composition and evolution of carbon dust. *The Astrophysical Journal*, 415:250–257, 1993.
- [6] F. Calvo, S. Tran, S. A. Blundell, C. Guet, and F. Spiegelmann. Three-dimensional global optimization of na_n^+ sodium clusters in the range $n \lesssim 40$. *Phys. Rev. B*, 62:10394–10404, Oct 2000.
- [7] Jan Cami, Jeronimo Bernard-Salas, Els Peeters, and Sarah Elizabeth Malek. Detection of c60 and c70 in a young planetary nebula. *Science*, 329:1180–1182, 2010.
- [8] F. Javier Dominguez-Gutierrez, Predrag S. Krstic, Stephan Irle, and Remigio Cabrera-Trujillo. Low-energy hydrogen uptake by small-cage c_n and c_{n-1} b fullerenes. *Carbon*, 134:189, 2018.
- [9] BT Draine and Aigen Li. Infrared emission from interstellar dust. i. stochastic heating of small grains. *The Astrophysical Journal*, 551(2):807, 2001.
- [10] M. Elstner, D. Porezag, G. Jungnickel, J. Elsner, M. Haugk, T. Frauenheim, S. Suhai, and G. Seifert. Self-consistent-charge density-functional tight-binding method for simulations of complex materials properties. *Phys. Rev. B*, 58(11):7260–7268, Sep 1998.
- [11] Marcus Elstner and Gotthard Seifert. Density functional tight binding. *Phil. Trans. R. Soc. A*, 372(2011):20120483, 2014.
- [12] M. J. Frisch, G. W. Trucks, H. B. Schlegel, G. E. Scuseria, M. A. Robb, J. R. Cheeseman, G. Scalmani, V. Barone, B. Mennucci, G. A. Petersson, H. Nakatsuji, M. Caricato, X. Li, H. P. Hratchian, A. F. Izmaylov, J. Bloino, G. Zheng, J. L. Sonnenberg, M. Hada, M. Ehara, K. Toyota, R. Fukuda, J. Hasegawa,

- M. Ishida, T. Nakajima, Y. Honda, O. Kitao, H. Nakai, T. Vreven, J. A. Montgomery, Jr., J. E. Peralta, F. Ogliaro, M. Bearpark, J. J. Heyd, E. Brothers, K. N. Kudin, V. N. Staroverov, R. Kobayashi, J. Normand, K. Raghavachari, A. Rendell, J. C. Burant, S. S. Iyengar, J. Tomasi, M. Cossi, N. Rega, J. M. Millam, M. Klene, J. E. Knox, J. B. Cross, V. Bakken, C. Adamo, J. Jaramillo, R. Gomperts, R. E. Stratmann, O. Yazyev, A. J. Austin, R. Cammi, C. Pomelli, J. W. Ochterski, R. L. Martin, K. Morokuma, V. G. Zakrzewski, G. A. Voth, P. Salvador, J. J. Dannenberg, S. Dapprich, A. D. Daniels, Ö. Farkas, J. B. Foresman, J. V. Ortiz, J. Cioslowski, and D. J. Fox. Gaussian09 Revision A.1, 2009. Gaussian Inc. Wallingford CT 2009.
- [13] D. A. García-Hernández, N. Kameswara Rao, and D. L. Lambert. ARE C-60 MOLECULES DETECTABLE IN CIRCUMSTELLAR SHELLS OF R CORONAE BOREALIS STARS? *The Astrophysical Journal*, 729:126, 2011.
- [14] D. A. García-Hernández, A. Manchado, P. García-Lario, L. Stanghellini, E. Villaver, R. A. Shaw, R. Szczerba, and J. V. Perea-Calderon. FORMATION OF FULLERENES IN H-CONTAINING PLANETARY NEBULAE. *The Astrophysical Journal Letters*, 724:L39, 2010.
- [15] DA García-Hernández, S Iglesias-Groth, JA Acosta-Pulido, A Manchado, P García-Lario, L Stanghellini, E Villaver, Richard A Shaw, and F Cataldo. The formation of fullerenes: Clues from new c60, c70, and (possible) planar c24 detections in magellanic cloud planetary nebulae. *The Astrophysical Journal Letters*, 737(2):L30, 2011.
- [16] Domingo Aníbal García-Hernández, Eva Villaver, Pedro García-Lario, José Antonio Acosta-Pulido, Arturo Manchado, Letizia Stanghellini, Richard A Shaw, and Franco Cataldo. Infrared study of fullerene planetary nebulae. *The Astrophysical Journal*, 760(2):107, 2012.
- [17] T. Heine, M. Rapacioli, S. Patchkovskii, J. Frenzel, A. Koster, P. Calaminici, H. A. Duarte, S. Escalante, R. Flores-Moreno, A. Goursot, J. Reveles, D. Salahub, and A. Vela. *deMonNano*, <http://demon-nano.ups-tlse.fr/>, 2009.
- [18] David Lawrence Hill and John Archibald Wheeler. Nuclear constitution and the interpretation of fission phenomena. *Phys. Rev.*, 89:1102–1145, Mar 1953.
- [19] Bruce J Hrivnak, Kevin Volk, and Sun Kwok. 2-45 micron infrared spectroscopy of carbon-rich proto-planetary nebulae. *The Astrophysical Journal*, 535(1):275, 2000.
- [20] Frank Jensen. Polarization consistent basis sets: Principles. *J. Chem. Phys.*, 115:9113–9125, 2001.
- [21] B. Joalland, M. Rapacioli, A. Simon, C. Joblin, C. J. Marsden, and F. Spiegelman. Molecular dynamics simulations of anharmonic infrared spectra of [sipah] pi-complexes. *J. Phys. Chem. A*, 114:5846, 2010.
- [22] Seong Gon Kim and David Tománek. Melting the fullerenes: A molecular dynamics study. *Phys. Rev. Lett.*, 72:2418–2421, Apr 1994.
- [23] W. Krätschmer, Lowell D. Lamb, K. Fostiropoulos, and Donald R. Huffman. Solid C₆₀: a new form of carbon. *Nature*, 347:354–358, 1990.
- [24] Sun Kwok, Kevin Volk, and Peter Bernath. On the origin of infrared plateau features in proto-planetary nebulae. *The Astrophysical Journal Letters*, 554(1):L87, 2001.
- [25] Marie L. Laury, Matthew J. Carlson, and Angela K. Wilson. Vibrational frequency scale factors for density functional theory and the polarization consistent basis sets. *J. Comput. Chem.*, 33:2380–2387, 2012.
- [26] Edyta Malolepsza, Henryk A. Witek, and Stephan Irlle. Comparison of geometric, electronic, and vibrational properties for isomers of small fullerenes C-20-C-36. *J. Phys. Chem. A*, 111(29):6649, JUL 26 2007.
- [27] I Mayer. Charge, bond order and valence in the abinitio scf theory. *Chem. Phys. Lett.*, 97:270, 1983.

- [28] S. Plimpton. Fast parallel algorithms for short-range molecular dynamics. *J. Comp. Phys.*, 117:1–19, 1995.
- [29] D. Porezag, T. Frauenheim, T. Köhler, G. Seifert, and R. Kaschner. Construction of tight-binding-like potentials on the basis of density functional theory - application to carbon. *Phys. Rev. B*, 51:12947–12957, 1995.
- [30] M. Rapacioli, C. Joblin, and P. Boissel. Spectroscopy of polycyclic aromatic hydrocarbons and very small grains in photodissociation regions. *Astronomy and astrophysics*, 429:193–204, 2005.
- [31] Mathias Rapacioli, Stéphanie Cazaux, Nolan Foley, Aude Simon, Ronnie Hoekstra, and Thomas Schlathölter. Atomic hydrogen interactions with gas-phase coronene cations: hydrogenation versus fragmentation. *Phys. Chem. Chem. Phys.*, 20:22427–22438, 2018.
- [32] Mathias Rapacioli, Fernand Spiegelman, Dahbia Talbi, Tzonka Mineva, Annick Goursot, Thomas Heine, and Gotthard Seifert. Correction for dispersion and coulombic interactions in molecular clusters with density functional derived methods: Application to polycyclic aromatic hydrocarbon clusters. *The Journal of chemical physics*, 130:244304, 2009.
- [33] Biswajit Saha, Stephan Irle, and Keiji Morokuma. Formation mechanism of polycyclic aromatic hydrocarbons in benzene combustion: Quantum chemical molecular dynamics simulations. *J. Chem. Phys.*, 132:224303, 2010.
- [34] Biswajit Saha, Sho Shindo, Stephan Irle, and Keiji Morokuma. Quantum Chemical Molecular Dynamics Simulations of Dynamic Fullerene Self-Assembly in Benzene Combustion. *ACS Nano*, 3:2241, 2009.
- [35] Kris Sellgren, Michael W Werner, James G Ingalls, JDT Smith, TM Carleton, and Christine Joblin. C60 in reflection nebulae. *The Astrophysical Journal Letters*, 722(1):L54, 2010.
- [36] A. Simon, J. P. Champeaux, M. Rapacioli, P. Moretto Capelle, F. X. Gadéa, and M. Sence. Dissociation of polycyclic aromatic hydrocarbons at high energy: MD/DFTB simulations versus collision experiments. *Theo. Chem. Acc.*, 137:106, 2018.
- [37] A. Simon, J. A. Noble, G. Rouaut, A. Moudens, C. Aupetit, C. Iftner, and J. Mascetti. Formation of coronene: water complexes: FTIR study in argon matrices and theoretical characterisation. *Phys. Chem. Chem. Phys.*, 19:8516, 2017.
- [38] A. Simon, M. Rapacioli, G. Rouaut, G. Trinquier, and F. X. Gadéa. Dissociation of polycyclic aromatic hydrocarbons: molecular dynamics studies. *Phil. Trans. Roy. Soc. A*, 375:20160195, 2017.
- [39] Aude Simon, Mathias Rapacioli, Joelle Mascetti, and Fernand Spiegelman. Vibrational spectroscopy and molecular dynamics of water monomers and dimers adsorbed on polycyclic aromatic hydrocarbons. *Phys. Chem. Chem. Phys.*, 14(19):6771, 2012.
- [40] Aude Simon and Fernand Spiegelman. Conformational dynamics and finite-temperature infrared spectra of the water octamer adsorbed on coronene. *Comput. Theor. Chem.*, 1021:54, 2013.
- [41] Aude Simon and Fernand Spiegelman. Water clusters adsorbed on polycyclic aromatic hydrocarbons: Energetics and conformational dynamics. *J. Chem. Phys.*, 138:194309, 2013.
- [42] A.G.G.M. Tielens. Interstellar polycyclic aromatic hydrocarbon molecules. *Annual Review of Astronomy and Astrophysics*, 46(1):289–337, 2008.
- [43] Henryk A. Witek, Stephan Irle, Guishan Zheng, Wibe A. de Jong, and Keiji Morokuma. Modeling carbon nanostructures with the self-consistent charge density-functional tight-binding method: Vibrational spectra and electronic structure of c-28, c-60, and c-70. *J. Chem. Phys.*, 125:214706, 2006.
- [44] T. W. Yen and S. K. Lai. Use of density functional theory method to calculate structures of neutral carbon clusters C_n ($3 \leq n \leq 24$) and study their variability of structural forms. *J. Chem. Phys.*, 142(8):084313, 2015.

- [45] GS Zheng, S Irle, and K Morokuma. Performance of the DFTB method in comparison to DFT and semiempirical methods for geometries and energies Of C-20-C-86 fullerene isomers. *Chem. Phys. Lett.*, 412(1-3):210, AUG 25 2005.

A Benchmark of IR spectra and correction factors

A.1 Systematic determination of correction factors

The vibrational modes of carbon clusters are poorly known, except for a few exceptions such as buckminsterfullerene. Here we use density-functional theory with the B3LYP functional and the pc-1 basis set [20] as the reference method. Being aware that this approach is not exact, all frequencies obtained with it are scaled by the appropriate factor of 0.973 [25].

A sample of 50 isomers of C_{24} were chosen randomly among those pertaining to similar families as the four reported in the present paper (the work on C_{24} where these families are described will be detailed elsewhere). Each isomer was locally reoptimized at the DFT/B3LYP/pc-1 level of theory, the normal modes being determined by standard diagonalization of the mass-weighted Hessian matrix. DFT calculations were performed with the Gaussian09 suite of programs [12]. This was not achieved for C_{60} isomers due to the evident too high computational cost at the DFT level. However, the peculiar but well known buckminsterfullerene isomer of C_{60} was added to the sample. Correlations between the frequencies obtained with the two methods (DFTB vs DFT) can be seen for a subset of particularly active modes in Fig. 3.

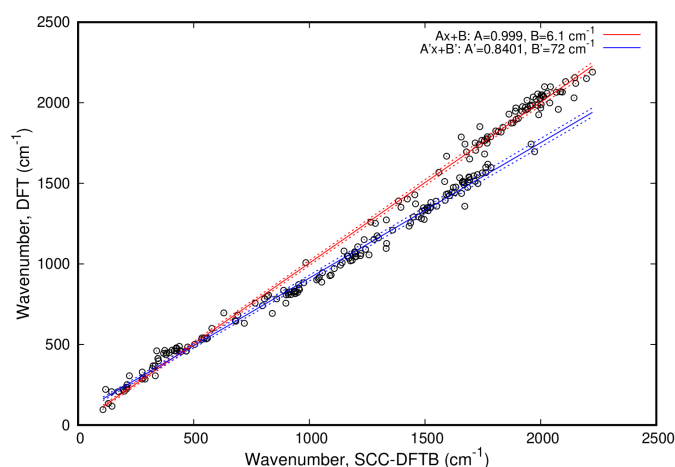


Figure 3: Harmonic line positions obtained at the DFT/B3LYP/pc-1 level of theory against the corresponding values with the SCC-DFTB method, for a sample of IR active modes from 51 isomers. The dotted lines above and below the main lines illustrate the corresponding uncertainties on each of the linear least-square fits.

This correlation plot displays two main linear regions, depending on whether the active mode lies below 1750 cm^{-1} or above this approximate threshold. The DFT frequencies are recovered from SCC-DFTB frequencies if linear relationships of the type $\sigma_{\text{DFT}} = A\sigma_{\text{DFTB}} + B$ are used in the corresponding ranges.

Least-square fitting procedures readily provide the following values for the linear coefficients, namely $A = 0.8401 \pm 0.0080$ and $B = 72 \pm 10\text{ cm}^{-1}$ for $\sigma_{\text{DFT}} < 1750\text{ cm}^{-1}$, and $A = 0.9990 \pm 0.0061$ and $B = 6.1 \pm 9.3\text{ cm}^{-1}$ for $\sigma_{\text{DFT}} > 1750\text{ cm}^{-1}$.

From the knowledge of the DFTB values, the IR band positions used to compare with astronomical spectra were determined using these linear relations, and further scaled by 0.973. For the sake of clarity, the uncertainty on the determined correction factors also shown in Fig. 3 was not applied to the spectra of Fig. 2.

A.2 Assessment of linear corrections on buckminsterfullerene and fully dehydrogenated coronene

The IR active modes of icosahedral C_{60} (buckminsterfullerene) and D_{6h} fully dehydrogenated coronene C_{24} were determined with the SCC-DFTB and DFT/B3LYP/pc-1 methods. The raw positions directly obtained with these methods are reported in Tables A.1 and A.2, along with the corrected SCC-DFTB values. For buckminsterfullerene, the residual shifts between corrected SCC-DFTB values and experimental data are also given.

Exp.	Raw B3LYP/pc-1	Raw SCC-DFTB	Corrected SCC-DFTB	Residual shift to exp.
18.9	18.7	19.8	20.7	+1.8
17.3	17.0	14.9	16.1	-1.2
8.5	8.3	7.1	8.3	-0.2
7.0	6.9	6.0	7.0	0.0

Table 1: Raw resonance wavelengths (in μm) of C_{60} buckminsterfullerene IR active normal modes at the DFT and SCC-DFTB levels. The corrected SCC-DFTB values are also mentioned, along with the corresponding shifts with respect to experimental data [23].

Raw B3LYP/pc-1	Raw SCC-DFTB	Corrected SCC-DFTB
24.2	29.0	28.4
21.8	21.4	22.1
12.4	11.0	12.3
9.5	8.2	9.4
6.5	5.8	6.8

Table 2: Raw resonance wavelengths (in μm) of dehydrogenated coronene C_{24} IR active normal modes at the DFT and SCC-DFTB levels. The corrected SCC-DFTB values are also mentioned.